

Programmable production of bioactive extracellular vesicles in vivo to treat myocardial infarction

Received: 16 April 2024

Accepted: 3 March 2025

Published online: 25 March 2025


 Check for updatesSiyuan Fu¹, Zhiyu Wang¹, Peihong Huang¹, Guanjun Li¹, Jian Niu¹, Zhiyang Li², Guangyue Zu³, Pengcheng Zhou⁴, Lianhui Wang¹, David Tai Leong⁵  & Xianguang Ding¹ 

Current myocardial infarction (MI) treatment strategies remain challenged in suboptimal pharmacokinetics and potential adverse effects. Here we present a bioelectronic interface capable of producing on-demand abundant bioactive extracellular vesicles (EVs) near the MI area for in-situ localized treatment. The technology, termed electroactive patch for wirelessly and controllable EV generation (ePOWER), leverages wireless bioelectronic patch to stimulate embedded electrosensitive macrophages, actively modulating the biosynthesis of EVs and enabling EV production with high programmability to be delivered directly to the MI area. ~2400% more bioactive EVs were produced per cell under our ePOWER system. When surgically implanted, we demonstrate the therapeutic potential of in-situ EV production system to alleviate MI symptoms and improve cardiac function. This programmable ePOWER technology enables in-situ production of therapeutically rich EVs, thus reducing the need for exogenous cell expansion platforms and dedicated delivery, holding promise as a therapeutic all-in-one platform to treat various diseases.

Myocardial infarction (MI), characterized by myocardial ischemia and necrosis resulting from severe blockage or interruption of coronary artery blood supply, continues to pose a significant health challenge with severe prognostic implications^{1,2}. Despite notable advancements that have been achieved, the limited regeneration capacity of myocardial tissue after MI leads to low rates of successful treatment³. This, combined with the rising incidence of younger-onset MI in recent years^{4,5}, severely exacerbates the challenge to public health. Traditional therapeutic strategies, such as thrombolytic agents, antiplatelet drugs and antithrombin, have been the cornerstone of MI management. However, these treatments are not without drawbacks, including the potential for significant complications like increased bleeding

risk and, in the case of antiplatelet medications like aspirin, the necessity for long-term administration which carries its inherent set of risks and challenges.

To improve therapeutics with mitigated side effects, cell therapy utilizing functional cells to enhance cardiac function and promote myocardial regeneration has emerged as a promising avenue for MI treatment⁴⁻⁹. Recent studies have showcased the efficacy of functional cell implantation in reducing infarct size, particularly in animal models¹⁰. Yet, the therapeutic potential of these strategies is often limited by the impaired migratory capacity of cells in the ischemic or inflamed myocardial environment and the inherent risks associated with cell transplantation^{11,12}, such as tumorigenesis and immune

¹State Key Laboratory of Flexible Electronics (LoFE) & Jiangsu Key Laboratory for Biosensors, Institute of Advanced Materials (IAM), Nanjing University of Posts and Telecommunications, Nanjing 210023, China. ²Department of Clinical Laboratory Medicine, Nanjing Drum Tower Hospital, Affiliated Hospital of Medical School, Nanjing University, Nanjing 210008, China. ³CAS Key Laboratory of Nano-Bio Interface, Suzhou Institute of Nano-Tech and Nano-Bionics, Chinese Academy of Sciences, Suzhou 215123, China. ⁴Department of General Surgery, Affiliated Hospital of Nantong University, Nantong 226001, China. ⁵Department of Chemical and Biomolecular Engineering, National University of Singapore, Singapore 117585, Singapore.  e-mail: cheltwd@nus.edu.sg; iamxgding@njupt.edu.cn

rejection^{13–15}. Hence, it is valuable to find cellular alternatives that could offer reliable therapeutic efficiency for MI treatment in vivo. Recent advances on intercellular communications demonstrated that cell therapy for MI may involve extracellular vesicles (EVs) engaging in near and long-distance paracrine signaling^{16–19}, of which play significant roles in reducing infarct volume and improving cardiac function. Leveraging this cellular surrogate could present a transformative, acellular opportunity to treat MI molecularly and at the organ level.

EVs are endogenously produced nanosized lipid bilayers packed with bioactive proteins, nucleic acids, and metabolites from their cells of origin^{20,21}, facilitating critical roles in intercellular signaling across various physiological and pathological processes^{22,23}. Compared to their derived cells, EVs offer unique advantages of low tumorigenicity and therefore confer higher biosafety for in vivo usage^{24,25}. Furthermore, located at the nanoscale range (ten to hundreds of nanometers), EVs are more likely to escape from general circulation, permeate compact tissues, making them an attractive alternative to traditional cell therapies^{26–29}. Recent studies on EV therapeutics have demonstrated that EVs not only enable similar therapeutic properties of their parental cells but also show potential in improving repairment outcomes of cardiovascular disease^{30,31}. Despite these promises, the clinical implementation of EV therapeutics remains challenging. Typically, producing EVs sufficient for therapeutic purposes is costly and labor-intensive, requiring complex procedures that challenge the scalability and consistency necessary for widespread clinical use³². Furthermore, the typical methods of administering EVs, such as intravenous injection, often result in rapid clearance from the body and suboptimal targeting of the affected myocardial tissue^{33,35}, limiting their efficacy in MI treatment. A number of studies have demonstrated that EVs are predominantly distributed to and accumulated in the liver after being injected intravenously^{35,36}. The actual dose of intravenously EV meaningfully reaching the MI region to even have a chance of exerting therapeutic is pessimistically low. Consequently, achieving the full therapeutic potential of EVs in MI management cannot be through present-day direct intravenous injection of exogenously produced EVs.

Motivated by recent discoveries on intracellular calcium ion pathways of EV biogenesis which can be regulated through electrical signals^{37,38}, here we propose and demonstrate a wireless implantable technology that enables electrically stimulating embedded electro-sensitive macrophages to produce bioactive EVs in vivo for MI therapy. Termed electroactive patch for wirelessly and controllable extracellular vesicle generation (ePOWER), the technology leverages bioadhesive cardiac patches containing integrated electronics that pass electrical signals to embedded electro-sensitive macrophages to accelerate the biosynthesis of EVs from these embedded with high controllability and programmability. M2-typed electro-sensitive macrophages known to produce therapeutic EVs to modulate homeostasis and promote tissue repair^{39,40}, were chosen as a proof of concept model for bioactive EV generation. ~2400% increase in EV yield could be achieved under ePOWER stimulation versus the conventional unstimulated cell culture control. The in-device in situ produced high abundance EVs also displayed anti-inflammatory properties on its own without any cross-talk with other cells. These anti-inflammatory EVs later facilitated the shift from the pro-inflammatory M1 phenotype to the reparative M2 phenotype of resident cardiac macrophages. Furthermore, these EVs showed diverse effects on cardiomyocyte proliferation, endothelial remodeling, and neo-angiogenesis. In a rat model of myocardial infarction, we demonstrated the therapeutic potential of the implanted in-situ EV production system to ameliorate inflammation, promote angiogenesis, and alleviate MI symptoms. As the EVs are produced on-demand, in situ and onsite, ePOWER does not suffer from any dilutive effect arising from vascular blood and the natural clearance via the liver but instead the as-produced EVs are directly therapeutically accessing the MI area.

Results

ePOWER technology

Our wireless on-demand EV-producing system was built on an electroactive cardiac patch embedded with M2-typed BV2 macrophages⁴⁰. The ePOWER system consists of a PEDOT:PSS flexible slim film that functions as a conductive layer to deliver electrical stimulation to loaded cells and an adhesive hydrogel that serves the dual purpose of fully encapsulating the patch and securely attaching the ePOWER patch to moist heart tissue (Fig. 1a). Microcircuits and micro battery devices were externally connected through wired connections, equipped with low-power wireless control modules to connect to electronic devices for the purpose of controlling electrostimulation modules (Supplementary Fig. 1).

Under the electro-stimulation of ePOWER patch, the encapsulated electrically sensitive BV2 experienced calcium influx, which enabled intracellular calcium signaling activation and finally led to an increment of EV production (Fig. 1b). The generated EVs exhibited anti-inflammatory characteristics, prompting the transformation of the pro-inflammatory M1 macrophage phenotype toward the healing M2 phenotype. Furthermore, these EVs manifested diverse effects on myocardial cell proliferation, endothelial cell migration, and angiogenesis, all of which benefit the therapeutic potential in regions affected by MI (Fig. 1c). The slim ePOWER patch can be implanted in a freely moving mouse with a close-fitting match against cardiac tissue interface (Fig. 1d, e). CT images clearly revealed the implanted ePOWER system in rat was wired connected to the MCU module cutaneously placed anterior to the heart (Fig. 1f). This enables wireless modulation of therapeutic EV production in vivo in a customizable and repeatable manner for treatment purposes.

In developing the ePOWER system, we developed self-gelling hydrogel as an adhesive layer of ePOWER patch to achieve robust adhesion adaptive to the complex motion behavior of the heart. The adhesive was first prepared as powder by mixing polyethyleneimine/polyacrylic acid/dopamine (DA/PEI/PAA) using a freeze-drying approach and then deposited on the patch surface (Fig. 2a)⁴¹. To prevent moisture evaporation and maintain adhesive performance, a non-adhesive silicone paper was applied to cover the ePOWER patch. In developing the adhesive, we designed and synthesized a panel of hydrogel with varying mass ratios to confer reliable attachment of the ePOWER patch. The self-gelling and adhesive DA/PEI/PAA complex formed crosslinked polymers on wet tissue in situ by absorbing interface liquid. It physically crosslinked through in-situ liquid absorption and established connections within the cross-linking framework composed of DA/PEI/PAA through intermolecular forces (Fig. 2b). To meet EV release across the cross-linked adhesive layer, low-molecular-weight of PEI (Mw, ca. 10,000) and PAA (Mw, ca. 3000) were selected. This selection ensures that the physical network of the cross-linked hydrogel layer wasn't excessively dense, of which potentially impedes the release of EVs⁴².

To determine the adhesive performance of the patch, shear experiments (Fig. 2c) were carried out on wet pig skin (Supplementary Fig. 2). Our dynamic testing revealed that DA_x/PEI_y/PAA_z with an optimized mass ratio of 1:5:5 showed the strongest adhesive performance, with adhesion stress of up to 58KPa (Fig. 2d, e). Under this optimized precursor ratio, the average zeta potential (-3.261 mV) and average pH (7.1) are in a relatively favorable range for maintaining the crosslinking density and low cytotoxicity (Supplementary Fig. 3). In addition, the storage modulus (G') of the adhesive was consistently lower than the loss modulus (G'') curve across the experimental duration, with the gap between the two moduli gradually decreasing, indicating a shift toward a gel-like behavior (Supplementary Fig. 4). Furthermore, the adhesive demonstrated a solid shear viscosity and thus exhibited a low fluidity state. The constant pressure shear assay indicated that the shear viscosity remains around 78 Pa·s within the

shear rate range of 0.1 to 1 s^{-1} (Fig. 2f), and the viscosity of the adhesive shows an increasing trend over time (Supplementary Fig. 5). These results indicated that DA₁/PEI₅/PAA₅ adhesive maintained a high viscosity and low flowability even when subjected to dynamic external force interference. This mechanical behavior makes it an ideal candidate to steadily attach ePOWER patch to beating heart tissue.

The adhesive hydrogel provided ePOWER additional encapsulation and current shielding. The voltage distribution of the conductive layer of the ePOWER patch showed uniformity and minimal voltage attenuation (Supplementary Fig. 6a). However, upon encapsulating the adhesive hydrogel, voltage strength markedly diminishes (Supplementary Fig. 6b). This configuration effectively prevented the direct impact of electrostimulation on the cardiac tissue. Scanning electron microscope (SEM) (Fig. 2g) demonstrated that the pore of the adhesive hydrogel was located at the micrometer size range (Supplementary Fig. 7), suitable for diffusing secreted EVs into the external environment. To support cell residence, L-arginine (L-Arg) was pre-modified on the conductive layer before adhesive hydrogel encapsulation to improve biocompatibility and immobilize cells. It was observed that after L-arginine functionalization (Fig. 2g, h), the patch showed advantaged cell growth without causing apparent cell toxicity within 7 days (Supplementary Fig. 8).

ePOWER promotes EV production

Using the established ePOWER system, we evaluated its EV generation capability. M2 macrophage cells BV2, an electrosensitive cell lines^{43,44}, were selected as proof of concept model cells seeded on ePOWER patch for EV production study. A specialized signal generator was employed to modulate the output direct current electrostimulation applied on embedded cells (Fig. 3a). EV-free FBS (dFBS) was employed in the cell culture (Supplementary Fig. 9). Transmission electron microscopy (TEM) was initially used to analyze and compare the generated EVs harvested from the supernatant of culture medium following various treatments (stimulation or not). These treatments produce two types of EVs: EV_{ePOWER}, derived from cells stimulated with ePOWER system, and EV_{Common}, derived from cells cultured under standard conditions without stimulation (Fig. 3b). It was found that the size of EV_{ePOWER} remained around 200 nm, with a characteristic cup-like shape. The morphology of EV_{ePOWER} remained intact, similar to natural EVs (Fig. 3c). Western Blot demonstrated the presence of typical EV protein marker CD63 and other specific vesicular markers (Alix, CD9, and TSG101) in both isolated EV_{Common} and EV_{ePOWER} (Fig. 3d). To further quantify the capacity of ePOWER system for EV production, we collected culture mediums and quantified enriched EVs through conventional nanoparticle tracking analysis (NTA) as well as bicinchoninic acid assay (BCA). The productivities of EVs from

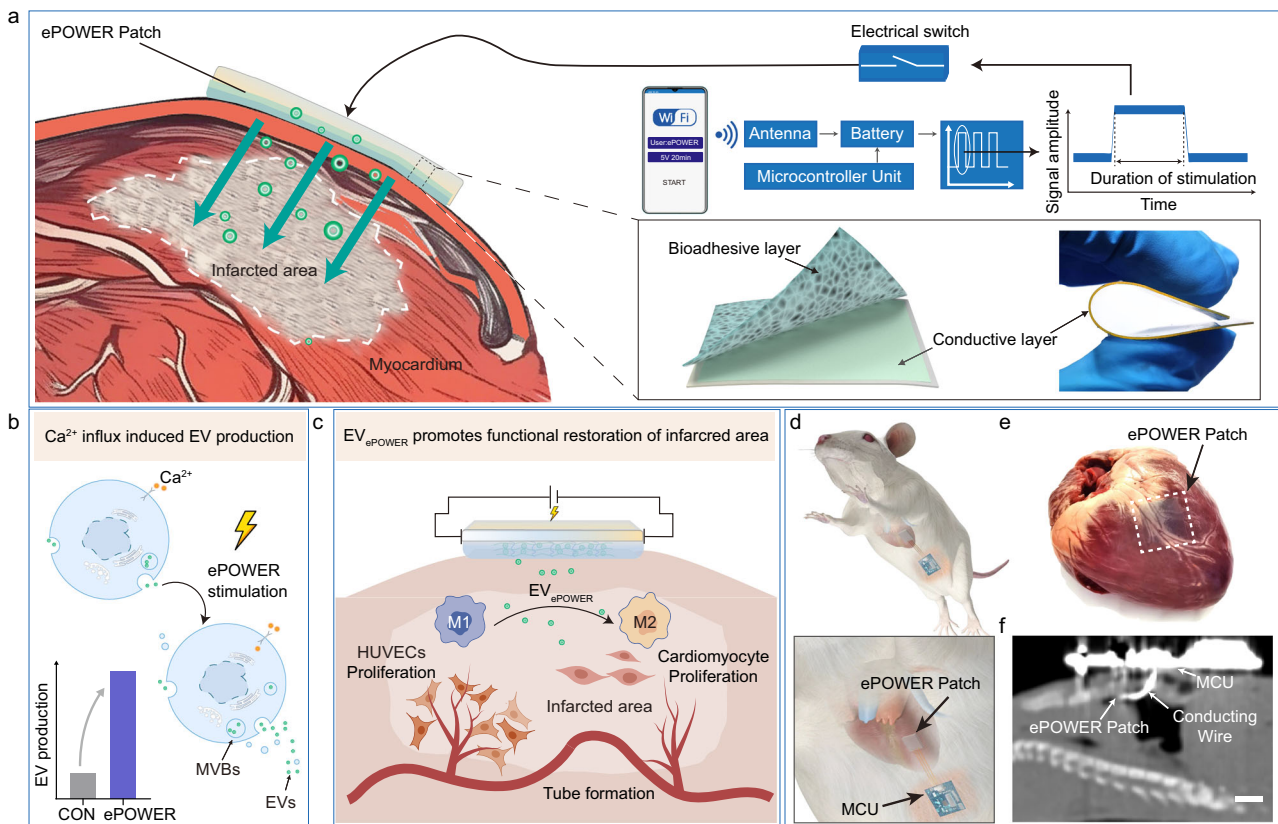


Fig. 1 | Schematic of implantable, flexible bioelectronics for MI treatment.

a Design of the implanted ePOWER patch system for electromodulated therapeutic extracellular vesicle (EV) production and in-situ therapy. Being attached to the impaired heart, ePOWER patch induces BV2 macrophages under load to produce bioactive EVs that improve cardiac repair. ePOWER system integrates an adhesive electroactive patch, a microprogramming control unit (MCU) module, and a WiFi antenna module to enable smartphone control of the treatment process. Insert: Schematic illustration of the implanted ePOWER patch consisting of a conductive layer and adhesive layer. By enabling the in-situ production of rich therapeutic EVs, the need for exogenous cell expansion platform, sufficient EV collection and delivery could be reduced, simplifying the therapeutic approach and leading to a

more straightforward and cost-effective method of treatment administration. **b** Schematic of ePOWER stimulus-inducible intracellular calcium ion influx and the activation of EVs biosynthesis. **c** Schematic of in-situ produced EV_{ePOWER} reprogramming MI-resident cardiac macrophages from M1 (that perpetuates inflammation in the MI area) to anti-inflammatory M2 phenotype, promoting cardiomyocyte proliferation, endothelial cell migration, angiogenesis and ultimately rescuing myocardial function and improving MI repair. **d** Rat implanted with the ePOWER patch system, with wired connection to the MCU module cutaneously placed anterior to the heart. **e** Optical image of ePOWER patch being fully covered on heart tissue. **f** Representative CT image of the implanted ePOWER system in rat (scale bars, 5 mm).

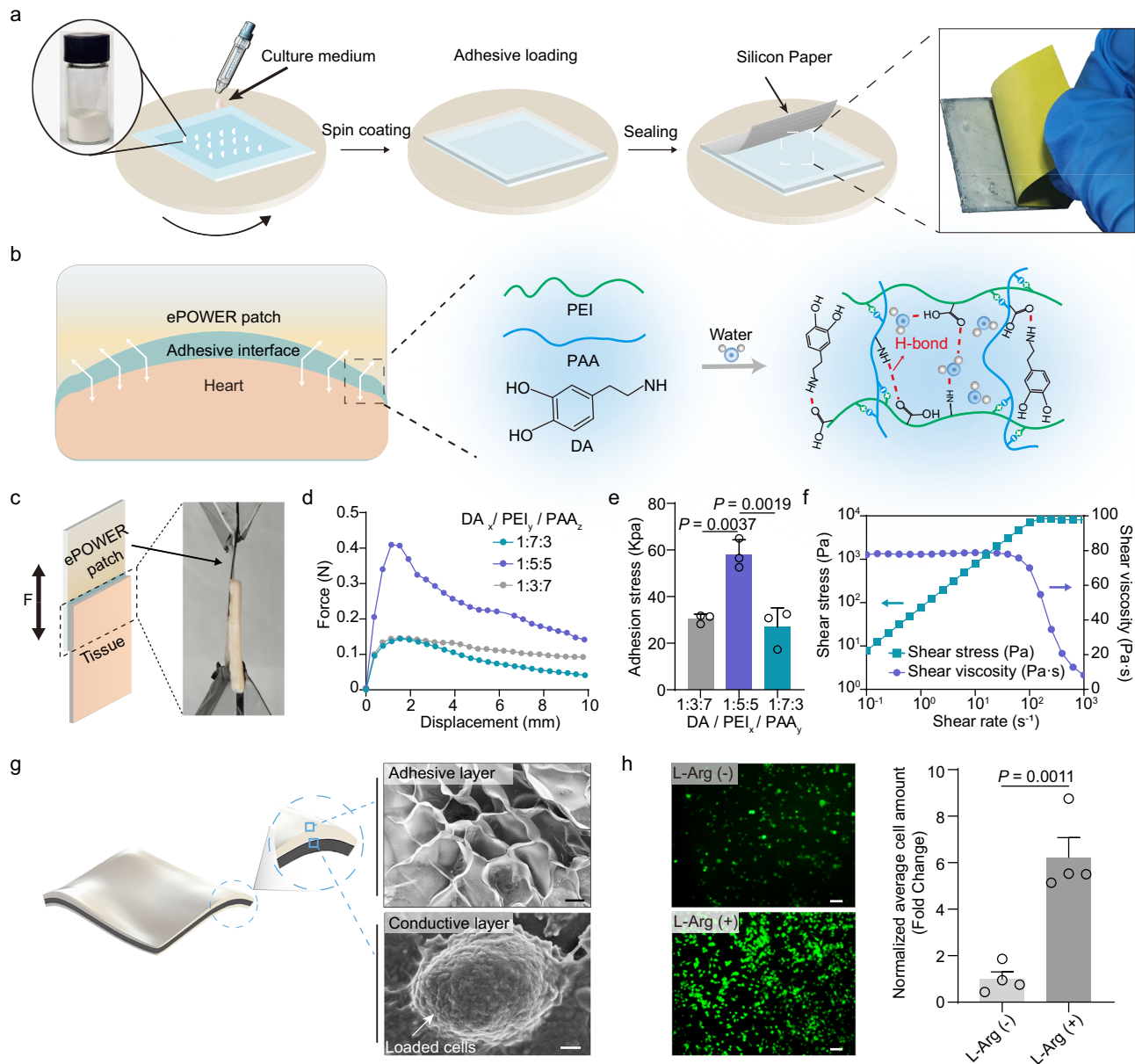
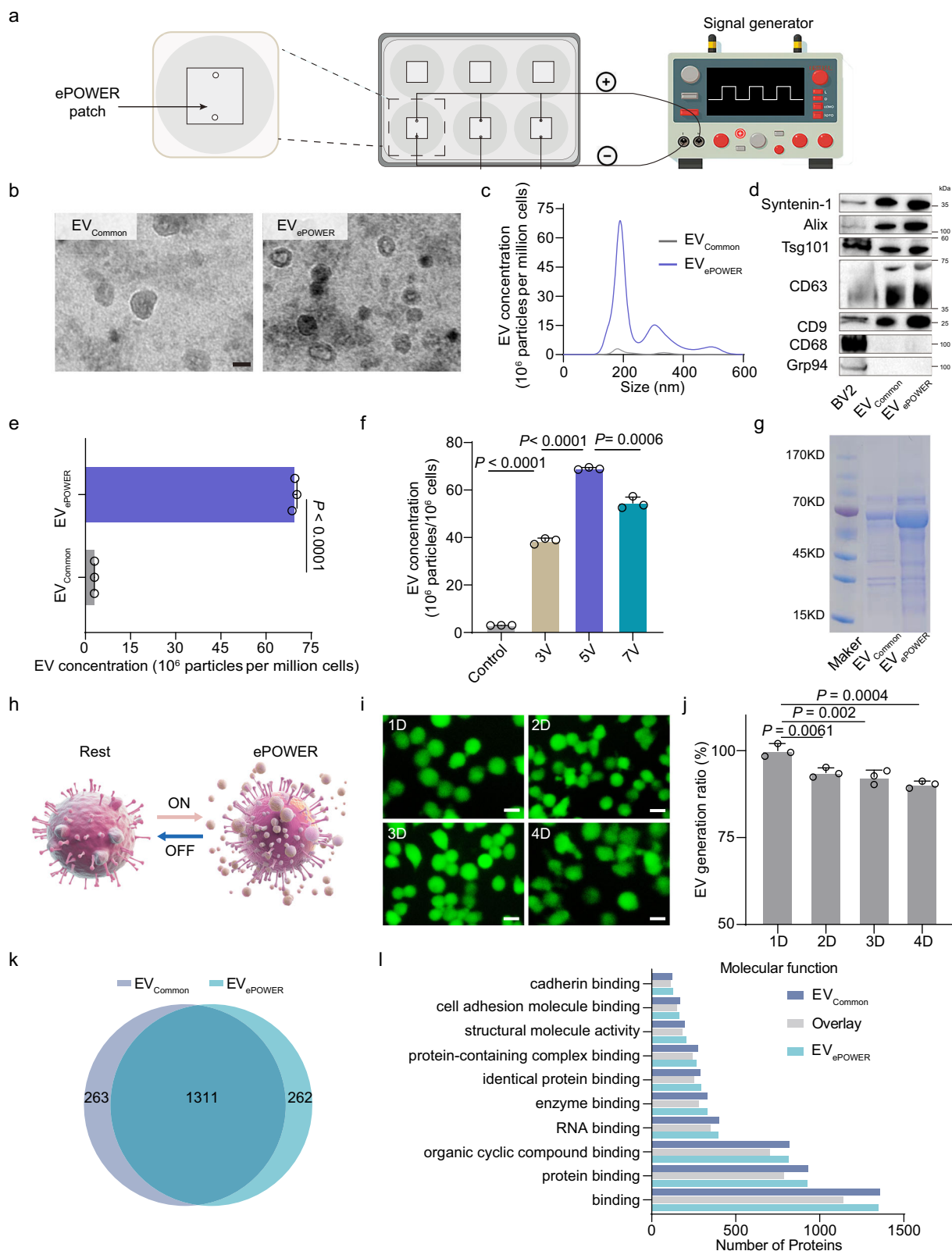


Fig. 2 | Adhesive ePOWER patch. **a** Schematic diagram illustrating the preparation of surface-loaded adhesive for ePOWER patches. Spin-coating method was employed to uniformly distribute the adhesive powder on the surface of ePOWER. Silicone paper was used to cover the ePOWER patch to prevent the adhesive from drying out. **b** The adhesive interface of ePOWER patch is primarily established by the physical crosslinking between PEI and PAA to create the principal framework, and the adhesion network was further established by dopamine with the inter-molecular force. **c** Schematic diagram and physical diagram of lap shear test. **d** The bonding strength of DA/PEI/PAA adhesive between wet tissue and membrane under different precursor ratios. **e** Adhesion stress of different DA/PEI/PAA adhesives on

wet tissues ($n = 3$). All tissues were soaked in cell culture medium (DMEM) at 37°C for 15 minutes before use. **f** Shear force and shear viscosity varied as a function of shear rate for the adhesive. **g** Scheme of ePOWER patch encapsulated with adhesive layer. Insert: SEM images of the adhesive layer (scale bars, 20 μm) and cells successfully loaded on the conductive layer (scale bars, 2 μm). **h** Viability of loaded cells on ePOWER substrate with and without L-arginine (Arg) modification (scale bars, 20 μm) ($n = 4$). Statistical differences were analyzed using one-way ANOVA with Turkey's multiple comparisons test. ns, not significant. The data is represented by an average of \pm SD.

different culture conditions were compared by normalizing obtained EVs against cell amounts. It was found that the number of EVs produced after electrostimulation was ~24 times higher than that of non-stimulated per cell counted (Fig. 3e). Through manipulating the applied voltages, the production of EVs was modifiable, with the optimal yield achieved at 5 V. Maintaining this voltage for 20 minutes resulted in the highest production yield of EVs (Fig. 3f and Supplementary Fig. 10). Under these parameter settings, the embedded cells did not show apparent damage (Supplementary Fig. 11). Given the good biosafety and high yield of EV generation, these settings were

selected in the following study of ePOWER for EV production. Next, we assessed if ePOWER-generated EVs possess protein profiles comparable to their counterparts. Based on the SDS-PAGE analysis, EV_{ePOWER} not only retained considerable protein composition across a wide range of sizes but also exhibited significantly greater protein signal (Fig. 3g), indicating a higher concentration of EV generated by ePOWER stimulation as compared to EV_{Common} obtained from untreated cells. To determine whether ePOWER systems could afford continuous and reliable EV production under repetitive stimulations, we measured the maintenance of EV production efficacy during kinetic

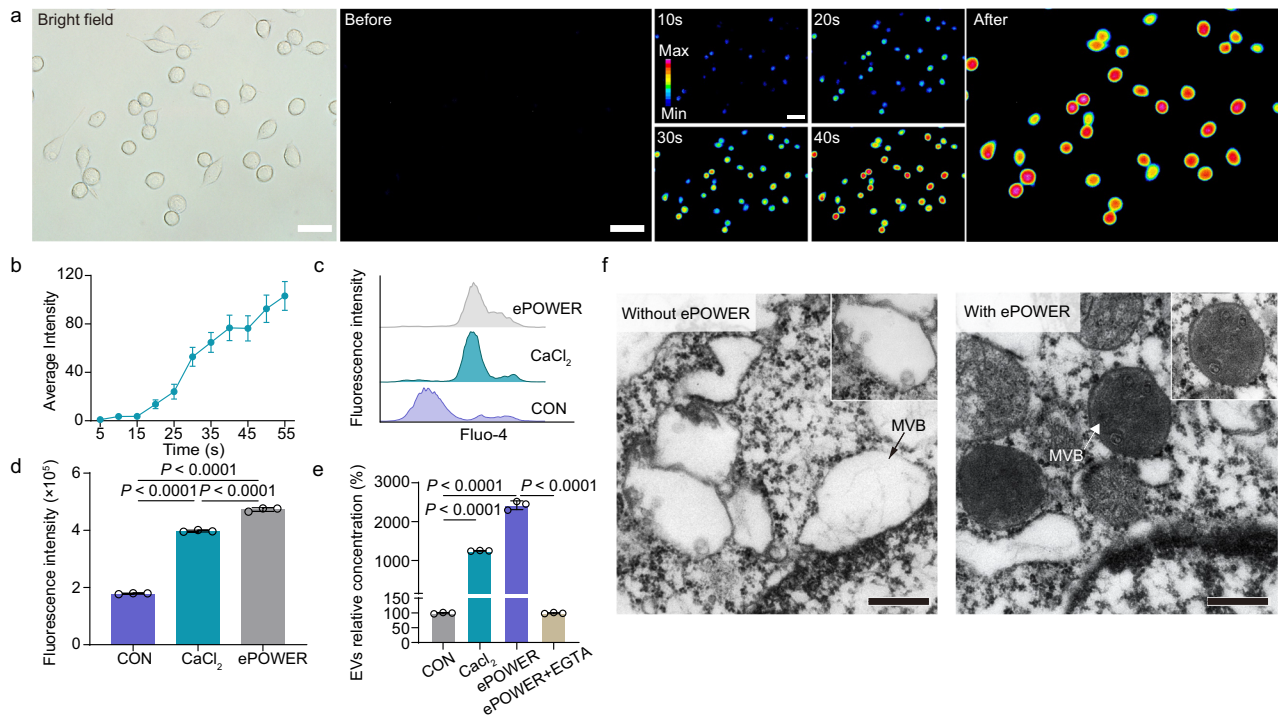


stimulations (Fig. 3h). Under safety stimulation conditions, the relative concentration of EV generated by ePOWER stimulation remained at a high level of above 80% within 4 days (Fig. 3i, j). These results indicated the capability of ePOWER to effectively promote EV generation without causing significant changes to their biochemical profiles. Collectively, these results support the use of ePOWER device as a reliable biosynthesis factory to produce bioactive EVs

from functional cells for therapeutic usage. Further proteomic studies have shown that EV_{Common} and EV_{ePOWER} shared a total of 1311 identical proteins (Fig. 3k). The identification and analysis of these proteins and their annotated biological processes, cellular components and molecular functions suggested considerably similar protein contents within EV_{Common} and EV_{ePOWER} (Fig. 3l and Supplementary Fig. 12).

Fig. 3 | ePOWER enables large quantities of EV production. **a** Schematic representation of ePOWER setup for EV production. BV2 macrophage cells were first seeded on ePOWER patch and then pulsed with alternate polarization. **b** Representative TEM images of EV_{Common} and EV_{ePOWER} (scale bars, 100 nm). **c** The concentration of EVs generated under ePOWER stimulation determined by NTA. **d** Western blot analysis of specific vesicular marker proteins (Synestin-1, Alix, Tsg101, CD63, CD9, CD68, Grp94) in EVs generated with and without ePOWER stimulation. **e** Quantitative comparison of EV concentrations generated under ePOWER stimulation and commonly cultured conditions ($n = 3$). Normalized against cell amounts. **f** EV yield under varying applied voltages and stimulation durations of the ePOWER system. The optimal yield was achieved at the condition of 5 V and 20 min ($n = 3$). **g** SDS-PAGE analysis of EVs obtained from M2 macrophages-embedded patch, either stimulate or not. **h** Schematic illustration of ePOWER enables repeatable EV

generation. **i** Viability of loaded BV2 macrophages on the substrate of ePOWER patch under continuous electrical stimulation for 4 days with one-day intervals (scale bars, 20 μm). **j** The relative concentration of EVs generated under ePOWER stimulation on different days. Above 80% of the production yield remained after 4 days' stimulation ($n = 3$). **k** Venn diagram to compare the EV_{ePOWER} and EV_{Common} proteins. **l** Biomass spectrometry identification analysis detected the number of proteins with corresponding molecular functions in EV_{ePOWER} (light blue) and EV_{Common} (dark blue). The proteins co-expressed by both are represented in gray. The EVs were obtained by differential centrifugation (First at 3000 g, then at 10,000 g and subsequently at 100,000 g for 2 hours). Statistical differences were analyzed using one-way ANOVA with Turkey's multiple comparisons test. The data is represented by an average of \pm SD.



between the treatments of CaCl₂, ePOWER, and the addition of EGTA plus ePOWER stimulation ($n = 3$). **f** Representative TEM images of cells with and without ePOWER stimulation. ePOWER stimulation leads to MVBs with more intraluminal vesicles (scale bars, 0.5 μm). Statistical differences were analyzed using one-way ANOVA with Turkey's multiple comparisons test. The data is represented by an average of \pm SD.

Mechanisms of ePOWER-regulated EV biosynthesis

Transient receptor voltage-gated calcium ion channel (Ca_v), which is abundantly expressed in various cells including electrosensitive BV2 macrophages, has recently gained significant attention for its role in modulating intracellular calcium signal transduction and EVs biosynthesis³⁵. By tuning calcium entry under electrostimulation, the intracellular calcium concentrations could be modulated to affect signal transduction and cell response³⁷. To explore the potential mechanism of ePOWER-elicited intracellular calcium ion waves and the related EV biogenesis, we then monitored the intracellular Ca²⁺ signal under ePOWER stimulation. The fluorescence results demonstrate that the Ca²⁺ gradually increases with the duration of electrostimulation (Fig. 4a, b). After 5 volts and 20 minutes of stimulation, ePOWER treatment significantly increased Ca²⁺ fluorescence in M2 BV2 macrophages, which was similar to CaCl₂ treatment control, indicating an influx of calcium ions into the cells during ePOWER stimulation (Fig. 4c, d). To further confirm whether the intracellular Ca²⁺ transients

following ePOWER stimulation account for the enhanced EV production, CaCl₂ was introduced into commonly cultured cells without ePOWER treatment. Indeed, we observed a substantial increase of EV production, exhibiting a maximum increase of over 20 times when compared to non-treatment control. In contrast, when the ePOWER stimulation was pretreated with ethylene glycol bis (2-aminoethyl ether) tetraacetic acid (EGTA), a typical Ca²⁺ chelating agent, the quantity of EVs was substantially decreased (Fig. 4e). These results suggest the key role of intracellular Ca²⁺ activity in ePOWER-mediated enhancement of EV production.

Moreover, the biogenesis of EVs involves the formation of multivesicular bodies (MVB) components, which were supposed to be sensitive to the intracellular calcium ion level⁴⁵. MVBs contain a large number of intraluminal vesicles (ILVs), serving as intracellular shuttles contributing to the following EV release. We next examined the changes in subcellular structure MVBs after ePOWER stimulus. TEM images revealed that ePOWER-stimulated cells generate more ILVs-

containing MVBs (Fig. 4f), which offers intuitive evidence for the substantial release of EVs following ePOWER-stimulation. Taken together, these findings indicated that the ePOWER is capable of inducing intracellular calcium ion signaling and regulating subcellular organelles, such as MVB, to facilitate abundant EV generation. It was noteworthy that the detailed mechanism of EV secretion under ePOWER stimulation is considerably more complex than intracellular calcium ion waves⁴⁶. Substantial work is still needed to elucidate the other effects, such as autophagy, to optimize and achieve a more efficient ePOWER system.

Enhancement of angiogenesis and myocardial cell proliferation in vitro

As an important constituent of the immune system, macrophages play a crucial role in managing inflammation following trauma or injury. Inflammation caused by MI can impede heart healing and accelerate necrosis. It was reported that repolarizing the inflammatory M1 phenotype of MI-resident (M1r) cardiac macrophages to the anti-inflammatory M2 phenotype could contribute to the restoration and regeneration of various tissues and organs⁴⁷. We then leveraged the M2 BV2 macrophages-seeded ePOWER system to produce EV_{ePOWER} and assess their influence on inflammatory M1 cardiac macrophage polarization. Additionally, we also collected commonly secreted EV_{Common} from M2 BV2 macrophages of equivalent cell culture number but were unstimulated as a control (Fig. 5a). After 24 hours of incubation, both EV_{Common} and EV_{ePOWER} led to morphological changes in macrophage, which involved the development of extended pseudopodia (Supplementary Fig. 13). These changes are typically associated with the M2 phenotype and confirmed the reprogramming of the M1r cardiac macrophages. Since the MI cardiac macrophages aggravate the inflammatory microenvironment at the infarct area, fast reprogramming induced by EV will flip the proinflammatory microenvironment of the MI area to an anti-inflammatory one. This fast flipping is necessary in setting the path towards post-MI recovery. During ePOWER stimulation, the M2 BV2 macrophages embedded on the ePOWER patch did not show any discernible polarization trend behavior (Supplementary Fig. 14), possibly due to the presence of dopamine molecules with anti-inflammatory catechol group in the patch⁴⁸. We further analyzed the typical M2 markers CD206 (Fig. 5b) and CD86 in macrophages (Supplementary Fig. 15). The result demonstrates that both EV_{Common} and EV_{ePOWER} promoted the repolarization of cardiac macrophages from M1 to M2 phenotype. We observed that EVs produced by ePOWER with a higher biogeneration amount show a stronger effect in promoting M2 polarization (Fig. 5c, d). Furthermore, in comparison to EV_{Common}, the EV_{ePOWER} treatment showed a higher expression level of anti-inflammatory factors, such as interleukin-10 (IL-10) and a decrease in the expression of proinflammatory factors like tumor necrosis factor- α (TNF- α), interleukin-1 β (IL-1 β), and interleukin-6 (IL-6) (Supplementary Fig. 16).

During the MI repair process, endothelial cells are essential in promoting angiogenesis, which improves the blood supply and oxygen delivery to benefit the ischemic area⁴⁹. We next investigated the effect of EV_{ePOWER} on endothelial cells, with a particular focus on migratability that is closely related to their angiogenesis potential⁵⁰. Using a transwell system, EV_{Common} and EV_{ePOWER} enriched from the equivalent amount of BV2 macrophages were introduced to the upper chamber and co-cultured with HUVECs for 24 hours. The results revealed that the EV_{ePOWER} showed significantly enhanced mobility of HUVECs compared to the other groups (Fig. 5e, f). Furthermore, a scratch assay was performed to evaluate the impact of produced EVs on the migratory behavior of endothelial cells. The results demonstrated a significant increase of cell migration distance or closure area in both two EV treatments, with a significantly higher cell migration rate in EV_{ePOWER} than EV_{Common} (Supplementary Fig. 17). Furthermore, a tube formation assay was used to assess how EV_{ePOWER} affects the

differentiation of endothelial cells. When comparing EV_{Common} with EV_{ePOWER}, both obtained from the supernatant of identical seeding cell amounts, EV_{ePOWER} demonstrated a more significant number of capillary tube structures formed. This angiogenic response exhibited a time-dependent correlation, with a more pronounced level of angiogenesis observed at 6 hours than at 3 hours (Fig. 5g). Quantitative analysis revealed that EV_{ePOWER} outperformed in the total vessel length, vessel percentage area, and junction number (Fig. 5h, i). Together, the collected EV_{ePOWER} demonstrated the highest quantity and complexity of blood vessel formation (Supplementary Fig. 18). We further investigated the functionality of two different strategies-originated EVs on cardiomyocytes. Cardiomyocytes are thought to be the fundamental functional units of the heart, playing a crucial role in the recovery of MI and its proliferation can facilitate the formation of new myocardial tissue, filling the defect caused by the infarcted area and promoting the reconstruction of the damaged myocardium⁵¹. Primary cardiomyocyte cultures were established and validated via immunofluorescence staining for the cardiac troponin T marker (Supplementary Fig. 19 and Supplementary Movie 1)⁵². We found two EVs both promote the proliferation of cardiomyocytes (Fig. 5j and Supplementary Fig. 20), highlighting the influence of BV2 macrophage cell-derived EVs on myocardial cell activity. This cardioprotective potential was further corroborated by the analysis of the BV2 M2 cell-secretome within the ePOWER platform (Supplementary Fig. 21). Additionally, EV_{ePOWER} demonstrated a more pronounced proliferation effect on myocardial cells compared to EV_{Common}, possibly due to the higher EV generation amount (Fig. 5k).

Implanted ePOWER therapy in rats with MI

We next evaluated the feasibility of implanted ePOWER to produce EVs in vivo for MI treatment. The MI model was established in Sprague-Dawley (SD) rats by ligating the left anterior descending coronary artery (LAD). Afterward, the MI rats were randomly divided into four treatment groups, including an MI control group (CON), an ePOWER patch electrostimulation treatment group (ePOWER), a clinical aspirin drug treatment group (APC), and a combined ePOWER and APC group (ePOWER+APC). BV2 macrophages-loaded ePOWER patches (diameter=5 mm) were surgically attached to the infarcted area of the moist myocardium (Supplementary Fig. 22). All treatments were applied immediately after establishing the MI model, with a 4-day interval between ePOWER stimulation and drug treatment. The animals were euthanized 28 days later after surgery, and their hearts were collected for histological analysis (Fig. 6a). The working parameters for ePOWER were set as the same settings employed in *in vitro* experiments (5V, 20 minutes). Under these settings, we observed a significant EV signal distributed throughout the heart tissue following ePOWER stimulation (Supplementary Fig. 23). These results suggested the successful activation of ePOWER system to produce EVs in vivo under wireless control.

Echocardiography was performed 4 weeks after LAD ligation. In the M-mode echocardiogram, untreated infarcted rat hearts exhibited severe attenuation of the anterior wall motion and delayed inactivation. These abnormal phenomena were alleviated in the ePOWER and APC groups, with similar overall effects. Interestingly, the rats treated with both ePOWER stimulation and aspirin showed the most significant improvement in anterior wall motion amplitude. Throughout the treatment period, the left ventricular ejection fraction (LVEF) of the LAD ligation rats in the control group significantly decreased. Consistent with the M-mode echocardiographic results, the treatment of ePOWER or APC showed some degree of functional improvement after the four-week treatment assessment. Whereas the combined treatment group demonstrated a more significant therapeutic improvement (Fig. 6b, c). Overall, the three different treatment strategies provided partial protection against the decline in myocardial function after LAD ligation and the combined treatment showed a

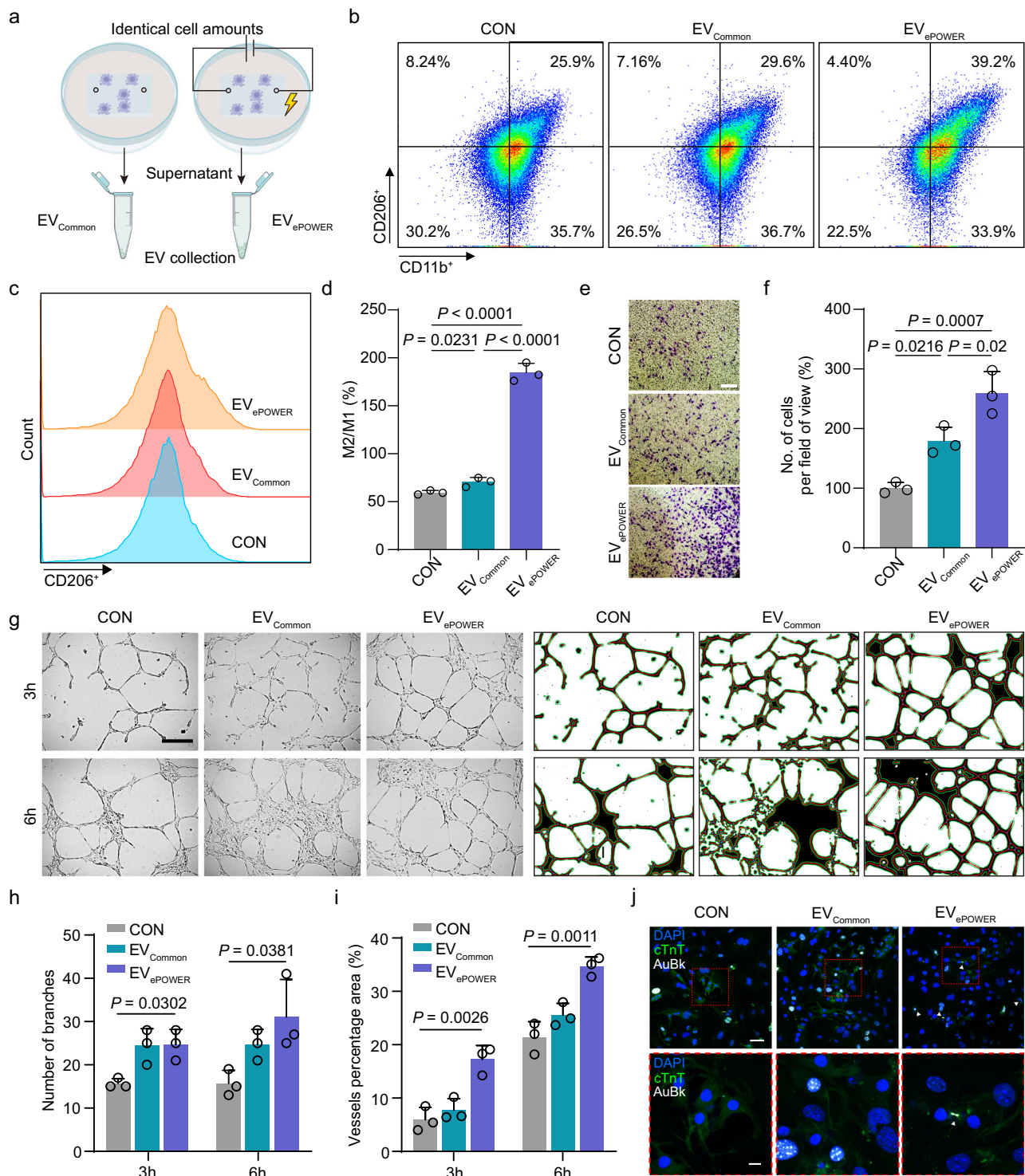


Fig. 5 | Functionality of macrophages-derived EV_{ePOWER} in vitro. **a** Schematic illustration of EVs collected from identically cultured cells with conventional culture condition or ePOWER stimulation condition. **b** Flow cytometry analysis of the phenotype of co-cultured macrophages treated with different-derived EVs. Typical M2 phenotypic marker CD206⁺ was employed for flow cytometry assay. **c** Quantification of CD206⁺ macrophages. **d** Quantification of the relative ratio of M2 macrophages to M1 macrophages ($n = 3$). **e** Representative images of the Transwell migration assay of HUVECs after EV treatments ($n = 3$). **f** Quantitative assay of the HUVEC migration ($n = 3$). **g** Left: Representative tube formation of

HUVECs with different EV treatments at 3 and 6 h. Right: Blood vessel image processed by ImageJ (scale bars, 100 μm). **h** Quantification of the number of vascular branches representing vascular formation capability in different EV treatment groups ($n = 3$). **i** Quantification of vessel percentage area in different groups ($n = 3$). **j** Proliferation of rat cardiomyocytes at 12 hours treated with various sourced (common culture strategy and ePOWER stimulus). Scale bar (top), 50 μm; scale bar (down), 10 μm. White arrows denote the presence of AuBk at the cell mid-body. Statistical differences were analyzed using one-way ANOVA with Tukey multiple comparisons test. The data is represented by an average of \pm SD.

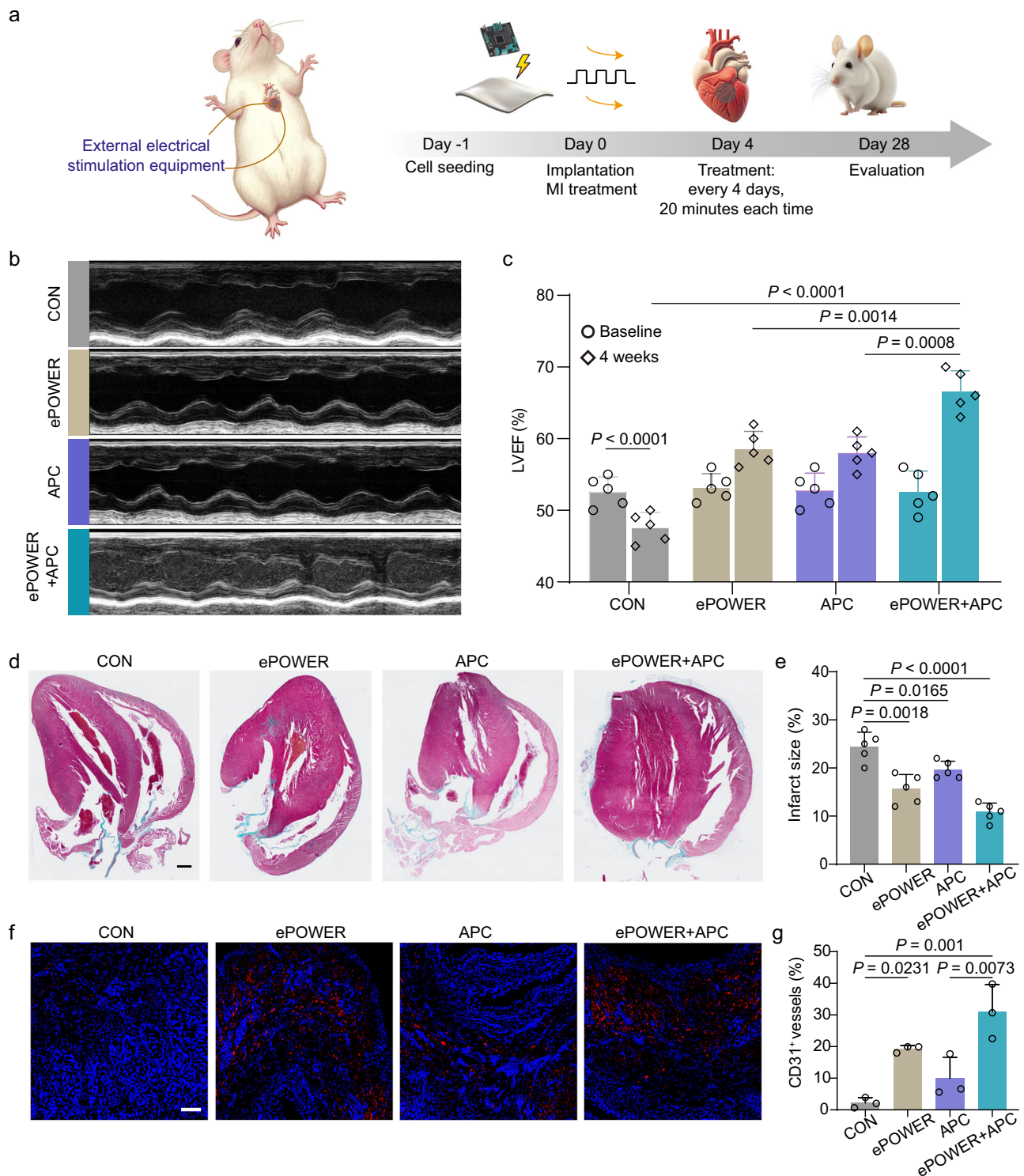


Fig. 6 | Implanted ePOWER therapy in rats with MI. **a** Schematic of the study design. After successful MI modeling, ePOWER was surgically implanted and treated accordingly. Echocardiography was performed 4 weeks after treatment. **b** Representative M-mode echocardiography images in each group after 4 weeks. **c** Quantification of LVEF percentage after 4 weeks of treatments ($n = 5$). **d** Representative MASSON staining of heart tissues in different groups (scale bar, 1 mm). **e** Quantification of the size of infarct areas after different treatments ($n = 5$).

f Representative angiogenesis staining of the infarct boundary area in different groups. Immunostained with anti-CD31 antibodies (blue: DAPI, red: CD31, scale bars, 100 μ m). **g** Quantification of the number of angiogenesis in the infarct boundary area in different groups ($n = 3$). Statistical differences were analyzed using one-way ANOVA with a Tukey multiple comparisons test. The data was represented by an average of \pm SD.

more favorable therapeutic effect for dynamic cardiac function recovery.

To further evaluate the therapeutic effect of ePOWER in MI animal models, the hearts of rats were dissected 28 days after surgery and

subjected to Masson's trichrome staining to assess myocardial fibrosis by detecting typical collagen protein content in fibrotic scars. Figure 6d shown the representative transverse cardiac sections from the mid-ventricular region. The untreated group exhibited significant blue

staining of fibrous connective tissue, with fibrous tissue replacing a substantial portion of the left ventricle. In contrast, the areas stained blue in the device treatment group and the drug treatment group were smaller. The quantified results revealed a more significant reduction in the combined treatment group, with an infarct area of approximately only 10% (Fig. 6e). This indicates a lower level of fibrosis in the infarcted area, consistent with the results obtained from M-mode echocardiography. To evaluate the angiogenic effect in the myocardial infarction (MI) region among each treatment group, we assessed the expression level of angiogenic protein marker CD31⁺. Compared to the control group (MI without treatment), the ePOWER stimulation group showed a substantially higher fluorescence of CD31⁺, suggesting enhanced angiogenesis. This increased angiogenesis could be further amplified when combined with clinical APC drug treatment (Fig. 6f, g).

To evaluate the potential systemic toxicity of ePOWER, histological examinations of major organs were conducted four weeks after treatment. Tissues from heart, liver, spleen, lungs, and kidneys from all treatment groups were collected for hematoxylin and eosin staining. The histological analysis suggested that the ePOWER patch did not cause noticeable side effects to normal organs (Supplementary Fig. 24). Additionally, blood routine tests and biochemistry revealed that all parameters in the ePOWER treatment groups were within normal ranges and comparable to those of the normal control group (Supplementary Figs. 25, 26).

Discussion

MI remains a major cause of mortality worldwide^{1,2}. The limited regenerative potential of myocardial cells under natural conditions results in a pronounced weakness in the heart's regenerative capacity when compared to tissues like the skin and liver. MI typically leads to sustained myocardial cell death due to the insufficient regenerative capability of these cells⁵³. This process often results in diminished heart function and, in severe cases, culminates in conditions such as heart failure, thus contributing to the generally suboptimal outcomes of MI treatments. Despite numerous attempts at cell therapies, regenerative strategies like stem cell therapy often grapple with issues of uncontrolled immunogenicity and potential tumorigenic risks^{13,14}.

To circumvent the inherent limitations of cell therapy, there has been a growing interest in using cell therapy derivatives (such as EVs) for MI treatment¹⁸. Multiple studies have demonstrated that EVs bear therapeutic properties akin to their parent cells and have the advantage of low tumorigenicity²⁵, making them promising candidates for improving MI repair. Nonetheless, EV therapy confronts challenges akin to cell therapy, encompassing hurdles in delivery to the intended site and the hindrance posed by the physiological metabolism, preventing effective accumulation within the treatment region³⁴. In this regard, a pivotal role is played by the continuous production and release of EVs within the treatment area. Cardiac patches have emerged as an effective delivery platform, though substantial scope remains for innovation to meet the demands of sustained EV production on such patches.

ePOWER system is a promising solution for the sustainable production and localized production of EVs in situ for MI treatment. By enabling the production of EVs directly at the injury site, the requirements for external cell expansion platforms, EV collection, and delivery could be reduced, streamlining the therapeutic process. This could lead to a more straightforward, less costly, and easier-to-administer treatment option. The ePOWER system incorporates wireless control modules and adhesive patches that facilitate EV generation, thus achieving programmable and controlled EV synthesis. This research showcased the applicability of this paradigm in MI treatment. Notably, the ePOWER system effectively diminishes infarct size, augments the thickness of the left ventricular wall, and fosters the proliferation of myocardial cells within high-risk regions of MI. Moreover, based on its inherent framework and design, the ePOWER system can facily tailor

EV generation to improve MI-related EV therapies further or branch out into addressing other maladies, for example, by loading different parental cells and modifying them through the electrical stimulation control module to match the needs of various cells in producing EVs (voltage, time, pulse waveform and so on).

To explore the possible bioactive components within EVs contributing to improved therapeutics, substantial work remains to be done to identify cargos and the potential differences in EVs undergoing ePOWER stimulation. In this proof of concept study, we utilized BV2 macrophages, which originate from the brain, due to their electrosensitivity and voltage-gated ion channels-key features that fit well with our study requirements for electrostimulated EV production. Additionally, these M2-typed BV2 cells also demonstrate anti-inflammatory and regenerative properties. The ePOWER patch leverages wireless bioelectronics to control and stimulate these electrosensitive macrophages, facilitating the localized production of bioactive EVs that support anti-inflammatory and regenerative effects at the site of myocardial injury. However, for future pre-clinical studies, more clinically accessible macrophages would be necessary. We have also acknowledged the potential benefits of incorporating other cell types, such as cardiac macrophages, cardiomyocytes, or MSCs, into the patch and benefit cardiac tissue (Supplementary Fig. 27). Future research could explore engineering these functional cells with the expression of electric sensors like Cav1.1 and genetic transducing modules to enhance their responsiveness to the electrical signals generated by ePOWER, potentially accelerating the electric-genetic transduction processes that drive EV biogenesis. For clinical application in humans, the ePOWER patch could be implanted by using minimally invasive surgical techniques, such as thoracoscopy or a small thoracotomy, to apply it directly to the epicardial surface of the heart. These strategies are already well-established in cardiac surgery. The scalability of this approach is promising, with the patch production scalable through established methods like electrospinning or 3D bioprinting, ensuring consistent quality.

Overall, this versatile approach may be extended to various realms of EV therapy, encompassing not only acute situations like MI but also chronic with much longer therapeutic runways diseases like diabetes, repair of acute spinal cord injuries, and even interventions within the realm of anti-cancer treatments⁵⁴⁻⁵⁸. Even in systemic scale delivery, this patch can also be patched on the skin, and the as-produced EV can enter the vasculature for body-wide distribution via nanomaterials-induced endothelial leakiness strategies^{59,60}. Given this perspective, the ePOWER system's potential applications within EV therapy span a wide spectrum.

Methods

Ethics statements

All live animal experiments were conducted under the guidance of the Academic Ethics and Ethics Committee of Nanjing University of Posts and Telecommunications (No: 202202).

Materials

Polyetherimide (PEI, Mw, ca.10,000, 9002-98-6), Dopamine (51-61-6), PEDOT: PSS (I55090-83-8), Polylysine (PLL, 25988-63-0), L-Arginine (74-79-3) were purchased from Aladdin. Polyacrylic acid (PAA, Mw, ca.3,000, 9003-01-4) was purchased from Sinopharm Chemical Reagent Co.Ltd. Anti-syntenin-1 (ab315342 1:1000), Anti-Alix (ab275377 1:1000), Anti-TSG101 (ab125011 1:1000), Anti-CD63 (ab217345 1:1000), Anti-CD9 (ab307085 1:1000), Anti-CD68 (ab303565 1:1000) were purchased from Abcam. Anti-GRP94 (2104 1:1000) was purchased from CST.

Preparation and characterization of ePOWER patch

For preparing PEDOT: PSS thin patch electrode, a 100 μ L solution of PEDOT: PSS was spin-coated onto the substrate at a rotation speed of

6000 rpm for 60 seconds. Subsequently, annealing was conducted at 150 °C for 20 minutes. The prepared thin patch electrode was then placed in a 2 mg/mL poly-L-lysine (PLL) solution overnight for modification. After the PLL modification, the thin patch electrode underwent ultraviolet (UV) sterilization. After that, the modified electrode was placed in a culture dish for cell incubation. The substrate preparation and PEDOT: PSS patch fabrication throughout the process were carried out in a clean room with controlled humidity, typically not exceeding 45%. A strict humidity control environment of 30-40% was maintained to prevent excessive water absorption by PSS. This practice aimed to enhance the repeatability and comparability of the fabricated devices. To further enhance the electrical conductivity of PEDOT: PSS, small amounts of additives such as dimethyl sulfoxide (DMSO), ethylene glycol, glycerol, sorbitol, sulfuric acid, or nitric acid were added to the PEDOT: PSS solution. These additives effectively altered the orientation of PEDOT chains, leading to improved electrical performance. The modified PEDOT: PSS thin patch electrode was then ready for cell incubation and subsequent experimentation.

We prepared a mixture of PEI (-10% by weight, Mw -10,000) and PAA (-10% by weight, Mw -3000) in an aqueous solution with a volume ratio of 3:7, 5:5, 7:3. Subsequently, we thoroughly mixed the 50 mL mixed solution by adding 1 mL of 5% dopamine hydrochloride saline solution. After that, the mixture was immersed in liquid nitrogen for -10 minutes and then subjected to freeze-drying in a freeze-drying machine for 48 hours. The resulting DA/PEI/PAA powder was obtained by grinding. Next, we mixed the DA/PEI/PAA powder with the cell culture medium to prepare the adhesive. The adhesive was uniformly dispersed in the desired loading area using the spin coating. After stabilizing the dispersed adhesive for 10 minutes, a layer of silicone paper was applied to prevent water evaporation. The silicone paper was removed at the time of use, and the adhesive patch was then affixed to the target area.

Wireless control system

The main modules of the wireless control system, including the wireless transmission unit, digital control logic, and power management, were designed based on ready-made components. The front end of the circuit mainly comprises a digital-to-analog converter (DAC) and a voltage conversion circuit, while the program was preset in the microprogramming control unit (MCU). The above circuit components mainly use commercial integrated ESP8266 modules (5×5 mm), and the built-in antenna adopts WiFi@2.4 GHz equipped with an external LOD regulator circuit module LMS1117, with a fixed output voltage of 3.3 V as its operating voltage. Moreover, Android-based dedicated control applications can be employed to set electrical stimulation parameters and wireless control can be achieved based on the WiFi module integrated within the MCU.

Voltage toxicity assay

In a new 6-well culture plate, one ePOWER patch was placed per well and 2 mL of culture medium was added to cultivate M2 microglia BV2 for 2 h (ePOWER patch was placed in 6-well culture plate and incubated with BV2 at 37°C for 2 h). DC signal generator was connected to the patch to output step voltage (0 V, 3 V, 5 V, 7 V, 9 V), respectively. After electrical stimulation, the myocardial cells were rinsed three times with PBS, and the cells were incubated with Calcein AM (1 μM) and Propidium iodide (1 μM) solution at 37°C for 30 minutes. Discard the staining solution, rinse PBS again three times, and observe the cells inside the device through a fluorescence-inverted microscope (Leica TCSSP8, Germany). Live cells were stained green, while dead cells were stained red. Randomly select 5 fields of view for each sample and calculate the average fluorescence intensity of living and dead cells, respectively. Calculate the cell survival rate according to the following formula:

[Average fluorescence intensity of living cells/ (Average fluorescence intensity of living cells + Average fluorescence intensity of dead cells)] × 100%. The fluorescence data obtained above were analyzed using ImageJ, and the voltage intensity suitable for stimulating cells was finalized.

Adhesive mechanical tests

The dynamic viscoelasticity of the adhesive was evaluated using a 5 mm diameter plate Rheometer (NETZSCH Kinexus Lab⁺). For the modulus/time experiment, the adhesive was subjected to a fixed strain of 1.0% and a frequency of 1 Hz, and the measurements were performed at room temperature. Additionally, frequency scanning experiments were conducted at room temperature, ranging from 0.1 Hz to 10 Hz, while maintaining a fixed strain of 1.0%. In the rotational/steady-state mode, the viscosity/time experiments were carried out at a fixed shear rate of 0.1 S⁻¹ and room temperature conditions. Subsequently, shear rate scanning experiments were performed, with shear rates ranging from 0.1 to 1000 s⁻¹. The final results were obtained by selecting logarithmic points based on the experimental data obtained from the Rheometer.

Cell culture

The BV2 microglia cells and H9C2 rat cardiomyocyte cells were plated in Dulbecco's modified Eagle's medium (DMEM) supplemented with 10% fetal bovine serum (FBS) and 1% Penicillin/ Streptomycin solution. Given the challenges associated with obtaining primary cardiac macrophages and the absence of a dedicated cardiac macrophage cell line, RAW 264.7 cells as model macrophages were used to study the phenomic dynamics of the cardiac macrophage. M1 macrophage was differentiated using 100 ng/mL LPS for 24 hours. HUVEC was cultured in endothelial cell culture medium (ECM) supplemented with 5% FBS, 1% penicillin Streptomycin, and 1% endothelial cell growth factor solution. The cell culture environment was maintained at a constant temperature of 37°C and 5% CO₂. The fresh culture medium was replaced every two days.

Isolation of primary rat cardiomyocyte cells

The primary rat cardiomyocytes were isolated following a previously reported method. In detail, the primary rat cardiomyocytes were isolated from the heart tissue of rats aged 1 days. After anesthetizing the rats, the hearts were excised and finely minced. The tissue fragments were washed by Hank's Balanced Salt Solution (HBSS) and then subjected to digestion with 1 mg/mL of type II collagenase (Gibco) solution at 37°C for 10 minutes. The digestion process was repeated 4-5 times. The supernatants were collected and centrifuged at 1,000 rpm for 5 minutes to collect the cells. The collected cells were pre-plated for 45 minutes twice to remove cardiac fibroblasts and enrich cardiomyocytes. Finally, the isolated rat cardiomyocytes were plated on 1% gelatine-coated Petri dishes and cultured in completed medium DMEM medium supplemented with 10% FBS for 4 days.

Cell cycle analysis

To evaluate the cell cycle of primary rat cardiomyocytes, cells were incubated with EV_{Common} or EV_{ePOWER} for 24 hours. Following the incubation, cells were fixed in 4% paraformaldehyde in PBS for 10 minutes, followed by permeabilization with 0.1% Triton X-100 in PBS for 5 minutes. The cells were then blocked with 5% BSA suspended in PBS for 1 hour and incubated with anti-Aurora B antibodies (ab2254) overnight at 4°C. Subsequently, the cells were washed by PBST thrice for 5 minutes and incubated with Alexa Fluor 647-conjugated secondary antibodies (ab150079) for 2 hours. The cells were washed by PBST thrice for 5 minutes and incubated with anti-cardiac Troponin T antibodies (CL488-26592, Proteintech) at 4°C overnight and then washed by PBST thrice for 5 minutes. Nuclei were stained with DAPI for

5 minutes. Fluorescence imaging was performed using an Olympus confocal microscopy (FV1000) with a 40× objective lens. Quantitative analysis was performed by calculating the proportion of cardiomyocytes with Aurora B expression in the midbody relative to the total number of cardiomyocytes.

Cytotoxicity evaluation in vitro

The adhesive mixture was dropped on the coverslip, and the coverslip was placed into a 6-well plate. Cells were seeded in a cell-cultured plate and incubated with DMEM for different times (1, 3, 5 and 7 days). Cells were stained with Calcein AM (1 μM) and Propidium iodide (1 μM) at 37°C for 30 minutes and fluorescence observation was performed using Olympus FV1000 confocal microscopy.

EV isolation and quantification

The ePOWER device containing M2 microglia BV2 was cultured in a vesicle-depleted medium (containing 5% vesicle-depleted FBS, dFBS). After one cycle of electrical stimulation, the medium was replaced with fresh dFBS medium and the cells were allowed to culture at 37°C for an additional 24 hours. We used differential centrifugation to isolate and concentrate EVs. First, all the culture supernatant was collected and centrifuged at 3000 g for 20 minutes to remove cell debris and larger particles. Then the cleared supernatant was subjected to 10,000 g for 30 minutes at 4°C. After that, the obtained solution was subjected to ultracentrifugation at 100,000 g for 2 hours at 4°C. The concentration of the obtained EVs was determined using nanoparticle tracking analysis (NTA, NanoSight NS300). To ensure optimal counting, the vesicle concentration was then fine-tuned to ~50 vesicles per field of view. EVs released at different voltage inputs (0, 3, 7 V) and input times (0, 10, 20, 30 minutes) were tested using the same method.

For the ELISA assay, 200 μL of the supernatant was collected and added to the enzyme-linked immunosorbent assay plate. The plate was incubated for 1 hour for adsorption, and the supernatant was aspirated. Subsequently, 1% bovine serum albumin (BSA) solution dissolved in PBS was added to each well and incubated for 1 hour to block non-specific binding sites. Blank wells were filled in this step. Then, the plate was gently tapped and blotted dry with lint-free paper to remove the excess liquid. Next, the plate was washed three times with 1× PBST buffer at pH 7.2–7.4. Each well was filled with the wash buffer during each wash step, and the plate was incubated for 3 to 5 minutes each time. Following the washing steps, 200 μL of cholesterol-modified horseradish peroxidase (HRP) was added to each well, and the plate was incubated for 1 hour. After incubation, the solution was removed, and the plate was washed three times, as described above. Then, 50 μL of substrate solution (TMB) and 30% H₂O₂ were added to each well, and the plate was incubated at room temperature in the dark for 10 minutes to initiate color development. Finally, after color development, 50 μL of stop solution (2 mol/L H₂SO₄) was added to each well to terminate the reaction. The optical density at 450 nm was measured using an ELISA reader.

Assessment of macrophage polarization in vitro

To evaluate the effect of EV_{ePOWER} on macrophage polarization, we co-cultured EV_{ePOWER} with macrophage. Specifically, macrophages (5×10⁴ cells/well) were inoculated in a 6-well plate and cultured overnight in DMEM containing 10% fetal bovine serum. Next, the same amount of PBS, EV_{Common} (4 μg/mL was around 2×10⁹ EV particle numbers per mL), and EV_{ePOWER} (100 μg/mL was around 5×10¹⁰ EV particle numbers per mL) were added to each well and incubated with the cells for 24 hours. The morphological changes of the macrophage were observed under an optical microscope. This allowed us to identify cell shape, size, and morphology changes following treatment with EV_{ePOWER}.

To evaluate the effect of EV_{ePOWER} on macrophage polarization, the macrophages were isolated from MI rats. The collected cells were incubated with anti-CD163 (MA5-16656, Invitrogen) at 4°C for

60 minutes and then incubated with secondary antibodies at 4°C for 60 minutes. The cells were washed with PBS for 5 minutes thrice and then incubated with anti-CD11b (201807, Biolegend) and anti-CD86 (200314, Biolegend) at 4°C for 20 minutes. Flow cytometry was used to detect changes in the content of M2 and M1 macrophages (Novocyte 2060).

ELISA

M1 macrophages were treated with PBS, EV_{Common}, and EV_{ePOWER} for 24 hours, respectively. The levels of tumor necrosis factor-alpha (TNF-α), interleukin-1β (IL-1β), interleukin-6 (IL-6), and interleukin-10 (IL-10) in culture medium were analyzed using ELISA kits from 4 A Biotech, China, following the vendor's instructions. All the quantification was conducted on a microplate reader (TECAN).

Transmission electron microscopy

EV_{Common} and EV_{ePOWER} were collected for TEM analysis using differential centrifugation and were resuspended in PBS. Then, 50 μL of EV solution was sucked onto the sealing patch. The ultra-thin copper mesh was placed on top of the droplet and left to stand for 20 minutes, during which EVs could attach to the copper mesh. Excess samples were carefully absorbed using the edge of filter paper. Next, 20 μL of the electron microscope fixed droplet was sucked onto the sealing patch. The copper mesh from the previous step was placed on the droplet and left for 5 minutes, allowing the electron microscope fixing solution to react with EVs. Excess samples were removed using filter paper. Under dark conditions, 20 μL of 1% uranyl acetate solution was absorbed into the sealing patch. The previous copper mesh was placed on the droplet for 10 minutes, ensuring sufficient reaction between EVs. Excess water was absorbed using filter paper. Finally, the copper mesh was dried at room temperature and observed under transmission electron microscopy (Hitachi, HT7700).

Scanning electron microscopy

The prepared adhesive condensate was dehydrated with gradient concentration alcohol (30%, 50%, 70%, 80%, 90%, 95%, 100%) by passing it through each alcohol concentration twice, each step lasting 15 minutes. After dehydration, the hydrogel was quickly frozen in liquid nitrogen for 5 minutes and then dried in a freeze-dryer for 12 hours. Subsequently, the vacuum-dried hydrogel sections were observed with a Scanning Electron Microscope (Hitachi, S-4800).

Western Blot

EV_{Common} and EV_{ePOWER} were collected and suspended in PBS. The isolated EVs were lysed using RIPA buffer (containing 1% Triton X-100, 1% NP-40, 0.1% SDS) and 1× protease inhibitor cocktail (Roche). The resulting lysate was incubated on ice for 10 minutes and then centrifuged at 16,000 g, 4 °C for 15 minutes. The protein concentration in the EV lysate was determined using the BCA protein quantification kit (Beyotime). Next, the proteins were separated by SDS-PAGE using polyacrylamide gels and subsequently transferred to PVDF membranes (Millipore Corp, Bedford, MA) through wet transfer at 300 mA for 1 hour. The PVDF membranes were blocked with 5% BSA at room temperature for 1 hour. Subsequently, the membranes were incubated overnight at 4 °C with the primary antibody (1:1000). After incubation, the membranes were washed thrice with TBST buffer for 10 minutes each time. Then, the membranes were incubated with the secondary antibody conjugated with HRP for 2 hours at RT. Signal detection was performed using the chemiluminescence method (ECL). The membranes were exposed to X-ray patches, and the images were captured using an image analyzer.

In-gel digestion

For in-gel tryptic digestion, the gel piece with a matched molecular mass of the targeted protein was excised and destained with 50%

acetonitrile in 50 mM ammonium bicarbonate (NH_4HCO_3). The destained gel piece was dehydrated with 100% acetonitrile for 5 minutes and incubated with 10 mM TCEP at 37 °C for 30 min. Then, the gel piece was again dehydrated with 100% acetonitrile and incubated with 25 mM iodacetamide at room temperature for 30 minutes in dark. After that, gel piece was washed with 50 mM NH_4HCO_3 and dehydrated with 100% acetonitrile. Finally, the gel piece was rehydrated and digested with 2 μg trypsin in 50 mM NH_4HCO_3 37°C overnight for protein in-gel digestion.

After digestion, peptides were extracted from the gel piece with 50% acetonitrile/0.1% formic acid. The extracted peptides were dried in SpeedVacuum concentrator and resuspended in 0.1% formic acid for LC-MS/MS analysis.

Calcium ion fluorescence image

Firstly, the cells were rinsed with PBS to remove the culture medium. Subsequently, a 1 μM fluo-4 AM calcium ion fluorescence probe was used to load the cells, and they were kept at 37°C for 30 minutes. Following the loading with Fluo-4, the cells underwent three washes with PBS. Then, the cells were electrically stimulated using electrodes while being observed under an inverted fluorescence microscope. For experiments involving drugs, the Fluo-4 loading process was carried out as described above. During the loading step, calcium chloride was added to achieve a final concentration of 6 μM , EGTA to achieve a final concentration of 5 mM, and benidipine to achieve a final concentration of 2 mg/mL. Fluorescence excitation of Fluo-4 was performed using a 470 nm LED with a 484/25 nm excitation filter. Observations were made through a 519/30 nm emission filter. Image acquisition was conducted at 10x magnification, with 50 ms of illumination every 1 second for a total of 240 seconds.

Flow cytometry analysis

Microglia (5×10^5 cells/well) were inoculated into 6-well plates, loaded onto ePOWER patches, and cultured overnight in DMEM containing 10% FBS. Each group of cells was incubated with the same amount of PBS, $\text{EV}_{\text{Common}}$, and $\text{EV}_{\text{ePOWER}}$. After 48 hours, microglia were collected and incubated with anti-CD11b APC-Cy7 (101216, Biolegend), anti-CD86 APC (105012, Biolegend), and anti-CD206-PE (141706, Biolegend) antibodies at 4°C for 30 minutes. Flow cytometry was used to detect changes in the content of M2 and M1 microglia (Novocyte 2060).

Transwell migration assay

Transwell assay was employed to evaluate HUVEC migration. HUVECs were suspended in serum-free ECM and seeded (1×10^5 per well) into the upper chamber of 24-well plates with an 8.0 μm polycarbonate membrane. The lower chamber was filled with a serum-free medium containing the same amount of PBS, $\text{EV}_{\text{Common}}$, and $\text{EV}_{\text{ePOWER}}$. Following 24 hours of incubation, the cells in the upper chamber were removed using a cotton swab; the migrated cells were stained with 0.5% crystal violet for 15 minutes and washed with PBS for 5 minutes thrice. Subsequently, the absorbance of each well was measured at 590 nm using a microplate reader, and the stained cell images were using an optical microscope.

Cell scratch assay

To assess the migration ability of HUVECs, we used the cell scratch method. First, HUVECs were inoculated into 6-well plates and incubated for 24 hours. Next, the wound would be scraped with a sterile straw head, washed the cells with PBS, and removed the unattached cells. The cells were then cultured in serum-free ECM and treated for 0, 12, and 24 hours under different groups. Finally, we captured images of the cells using an optical microscope and quantified the cell migration rate using ImageJ. The cell migration rate was calculated as the healed wound area/initial wound area \times 100%.

Tube formation assay

Tube-forming experiments were conducted to investigate the effect of $\text{EV}_{\text{ePOWER}}$ on angiogenesis in the MI region. First, Matrigel was placed in a refrigerator at 4 °C overnight 24 hours before use and thawed before use. We then used a pre-cooled pipette to add 50 μL of Matrigel to each well of a pre-cooled 96-well plate, which was then placed in a 37 °C, 5% CO_2 incubator for 1 hour until it solidified. Next, HUVECs (1×10^4 cells/well) were inoculated into the 96-well plates and treated with the same amount of PBS, $\text{EV}_{\text{Common}}$, and $\text{EV}_{\text{ePOWER}}$. The cells were then incubated for 3 and 6 hours, and images were captured using an optical microscope. ImageJ software was subsequently used for image analysis. The results of this analysis included the number of nodes, vessel percentage area, number of vascular branches and total length, providing a comprehensive assessment of various aspects of vascular formation.

Cell proliferation assay

The myocardial cells were incubated with the same amount of PBS, $\text{EV}_{\text{Common}}$, and $\text{EV}_{\text{ePOWER}}$ for 12 hours, respectively, and then transferred to a new 6-well culture plate. After rinsing them three times with PBS, the cells were treated with a cell staining solution consisting of 4 μM /L calcein AM and 1 μg /mL Hoechst 33342 in 4 milliliters of PBS. The plate was then placed in a cell culture incubator at 37 °C, 5% CO_2 , and saturated humidity for 30 minutes. Following the incubation period, the staining solution was discarded, and the cells were rinsed three times with PBS. The proliferation effect of the cells in the device was observed using a fluorescence-inverted microscope (Leica TCSSP8, Germany). To further analyze whether the proliferation of cardiomyocytes incubated with $\text{EV}_{\text{ePOWER}}$ in vitro is time-dependent, staining image acquisition was repeated at 4, 8, and 12-hour intervals after incubation. The obtained fluorescence images were analyzed using ImageJ, and the cell proliferation effect was evaluated based on the quantified fluorescence intensity.

Rat MI model and in vivo treatment

The MI model was performed on 10-week-old female Sprague Dawley rats after a 12-hour fast. The rats were placed in an induction box of an anesthesia machine and administered isoflurane to achieve deep anesthesia. Once the anesthesia was confirmed, the rats were placed in a supine position and secured to the operating table. The skin on the left side of the chest was sterilized prior to tracheal intubation. A left thoracotomy was performed at the third or fourth intercostal space using hemostatic forceps to open the intercostal space, and the coronary artery of the left anterior descending branch (LAD) was ligated entirely at the upper part of the LAD. The time for opening and ligation was limited to 15 seconds. Afterward, the chest was closed, and the rats were ventilated until they regained consciousness. The cardiac function of the rats was evaluated using an ultra-high-resolution small animal ultrasound imaging system (Vero 3100 LT). The heart was imaged through the instrument window, and cardiac function parameters, such as the left ventricular ejection fraction, were used to confirm the effectiveness of the modeling. After the model was established, the ePOWER device was surgically implanted. The ePOWER and ePOWER combined with APC group were treated with wireless signal (every 4 days, 20 minutes each time). Aspirin was administered to the rats via gavage at a dosage of 100 mg/kg/day. The administration began one day after the induction of myocardial infarction and continued daily throughout the study.

CT imaging

This device implants ePOWER patches into the heart of SD rats through surgery, with external circuits attached to the rat's body surface. After 7 days, SD rats were imaged using computed tomography (CT, nano-voxel I-2702E) to visualize the device location.

Echocardiography

The echocardiography experiment was conducted four weeks after successfully modeling MI and placing ePOWER for continuous echocardiography examination in rats. During the experiment, the rats were placed under light anesthesia (2% isoflurane) and imaged using a Ver0 3100 LT ultrasound system at a frequency of 21 MHz. M-mode images were recorded at the nipple level, and grayscale two-dimensional parasternal short-axis images were obtained for each rat. Measurements were performed in a blinded manner by a single observer. The amplitude of ventricular wall motion, the end-diastolic and end-systolic diameters of the left ventricle, and motor coordination were assessed based on the M-mode images. From these measurements, we calculated the left ventricular ejection fraction. Additionally, heart rate was determined from the M-mode images. Multiple consecutive shots were taken for each rat sample in the M-mode image.

Statistics and reproducibility

Statistical analysis was performed using GraphPad Prism software (v.8.0). Data were analyzed by one-way ANOVA (multiple comparisons) with Tukey's test and unpaired two-tailed t-test. All results were presented as mean \pm s.d. Unless otherwise stated, the experiments were independently conducted with at least three times for reproducibility of results.

Reporting summary

Further information on research design is available in the Nature Portfolio Reporting Summary linked to this article.

Data availability

All data are available in the main text or the supplementary materials. Source data are provided with this paper.

Code availability

The custom code used for the statistical analyzes is available from the corresponding author upon reasonable request.

References

- Tsao, C. W. et al. Heart disease and stroke statistics-2023 update: a report from the American Heart Association. *Circulation* **147**, e93–e621 (2023).
- Townsend, N. et al. Epidemiology of cardiovascular disease in Europe. *Nat. Rev. Cardiol.* **19**, 133–143 (2022).
- Bahit, M. C., Kochar, A. & Granger, C. B. Post-myocardial infarction heart failure. *JACC-Heart Fail* **6**, 179–186 (2018).
- Sagris, M. et al. Risk factors profile of young and older patients with myocardial infarction. *Cardiovasc Res* **118**, 2281–2292 (2022).
- Åberg, N. et al. Diverging trends for onset of acute myocardial infarction, heart failure, stroke and mortality in young males: role of changes in obesity and fitness. *J. Intern Med* **290**, 373–385 (2021).
- Tompkins, B. A. et al. Preclinical studies of stem cell therapy for heart disease. *Circ. Res* **122**, 1006–1020 (2018).
- Gao, L. et al. Exosomes secreted by hiPSC-derived cardiac cells improve recovery from myocardial infarction in swine. *Sci. Transl. Med* **12**, eaay1318 (2020).
- Sun, X. et al. Transplanted microvessels improve pluripotent stem cell-derived cardiomyocyte engraftment and cardiac function after infarction in rats. *Sci. Transl. Med* **12**, eaax2992 (2020).
- Park, B.-W. et al. In vivo priming of human mesenchymal stem cells with hepatocyte growth factor-engineered mesenchymal stem cells promotes therapeutic potential for cardiac repair. *Sci. Adv.* **6**, eaay6994 (2020).
- Zhu, D. et al. Minimally invasive delivery of therapeutic agents by hydrogel injection into the pericardial cavity for cardiac repair. *Nat. Commun.* **12**, 1412 (2021).
- Cheng, K. et al. Magnetic targeting enhances engraftment and functional benefit of iron-labeled cardiosphere-derived cells in myocardial infarction. *Circ. Res* **106**, 1570–1581 (2010).
- Terrovitis, J. V., Smith, R. R. & Marbán, E. Assessment and optimization of cell engraftment after transplantation into the heart. *Circ. Res* **106**, 479–494 (2010).
- Zhao, T., Zhang, Z.-N., Rong, Z. & Xu, Y. Immunogenicity of induced pluripotent stem cells. *Nature* **474**, 212–215 (2011).
- Deuse, T. et al. Hypoimmunogenic derivatives of induced pluripotent stem cells evade immune rejection in fully immunocompetent allogeneic recipients. *Nat. Biotechnol.* **37**, 252–258 (2019).
- Levy, O. et al. Shattering barriers toward clinically meaningful MSC therapies. *Sci. Adv.* **6**, eaba6884 (2020).
- Hodgkinson, C. P., Bareja, A., Gomez, J. A. & Dzau, V. J. Emerging concepts in paracrine mechanisms in regenerative cardiovascular medicine and biology. *Circ. Res* **118**, 95–107 (2016).
- Walter, J., Ware, L. B. & Matthay, M. A. Mesenchymal stem cells: mechanisms of potential therapeutic benefit in ARDS and sepsis. *Lancet Respir Med* **2**, 1016–1026 (2014).
- Vicencio, J. M. et al. Plasma exosomes protect the myocardium from ischemia-reperfusion injury. *J. Am. Coll. Cardiol.* **65**, 1525–1536 (2015).
- Saha, P. et al. Circulating exosomes derived from transplanted progenitor cells aid the functional recovery of ischemic myocardium. *Sci. Transl. Med* **11**, eaau1168 (2019).
- Mathieu, M., Martin-Jaular, L., Lavieu, G. & Théry, C. Specificities of secretion and uptake of exosomes and other extracellular vesicles for cell-to-cell communication. *Nat. Cell Biol.* **21**, 9–17 (2019).
- Van Niel, G., d'Angelo, G. & Raposo, G. Shedding light on the cell biology of extracellular vesicles. *Nat. Rev. Mol. Cell Biol.* **19**, 213–228 (2018).
- Valadi, H. et al. Exosome-mediated transfer of mRNAs and microRNAs is a novel mechanism of genetic exchange between cells. *Nat. Cell Biol.* **9**, 654–659 (2007).
- Yeung, C.-Y. C. et al. Circadian regulation of protein cargo in extracellular vesicles. *Sci. Adv.* **8**, eabc9061 (2022).
- Wiklander, O. P. B., Brennan, M. Á., Lötvall, J., Breakefield, X. O. & EL Andaloussi, S. Advances in therapeutic applications of extracellular vesicles. *Sci. Transl. Med* **11**, eaav8521 (2019).
- Xu, F. et al. Mesenchymal stem cell-derived extracellular vesicles with high PD-L1 expression for autoimmune diseases treatment. *Adv. Mater.* **34**, 2106265 (2022).
- Herrmann, I. K., Wood, M. J. A. & Fuhrmann, G. Extracellular vesicles as a next-generation drug delivery platform. *Nat. Nanotechnol.* **16**, 748–759 (2021).
- Li, Y. et al. Endothelial leakiness elicited by amyloid protein aggregation. *Nat. Commun.* **19**, 613 (2024).
- Qin, W. et al. Breaking through the basement membrane barrier to improve nanotherapeutic delivery to tumours. *Nat. Nanotechnol.* **19**, 95–105 (2024).
- Setyawati, M. I., Tay, C. Y., Bay, B. H. & Leong, D. T. Gold nanoparticles induced endothelial leakiness depends on particle size and endothelial cell origin. *ACS Nano* **23**, 5020–5030 (2017).
- Sahoo, S. et al. Therapeutic and diagnostic translation of extracellular vesicles in cardiovascular diseases: roadmap to the clinic. *Circulation* **143**, 1426–1449 (2021).
- Liu, B. et al. Cardiac recovery via extended cell-free delivery of extracellular vesicles secreted by cardiomyocytes derived from induced pluripotent stem cells. *Nat. Biomed. Eng.* **2**, 293–303 (2018).
- Wan, Y. et al. Rapid magnetic isolation of extracellular vesicles via lipid-based nanoprobables. *Nat. Biomed. Eng.* **1**, 0058 (2017).
- Gallet, R. et al. Exosomes secreted by cardiosphere-derived cells reduce scarring, attenuate adverse remodelling, and improve

- function in acute and chronic porcine myocardial infarction. *Eur. Heart J.* **38**, 201–211 (2017).
34. Wiklander, O. P. et al. Extracellular vesicle in vivo biodistribution is determined by cell source, route of administration and targeting. *J. Extracell. Vesicles* **4**, 26316 (2015).
35. Wiklander, O. P. B. et al. Extracellular vesicle in vivo biodistribution is determined by cell source, route of administration and targeting. *J. Extracell. Vesicles* **4**, 26316 (2015).
36. Kang, M., Jordan, V., Blenkinsop, C. & Chamley, L. W. Biodistribution of extracellular vesicles following administration into animals: a systematic review. *J. Extracell. Vesicles* **10**, e12085 (2021).
37. Messenger, S. W. et al. A Ca²⁺-stimulated exosome release pathway in cancer cells is regulated by Munc13-4. *J. Cell Biol.* **217**, 2877–2890 (2018).
38. Wu, H. et al. Accelerated intestinal wound healing via dual electrostimulation from a soft and biodegradable electronic bandage. *Nat. Electron* **29**, 1–4 (2024).
39. Li, Y. et al. Ultrasound controlled anti-inflammatory polarization of platelet decorated microglia for targeted ischemic stroke therapy. *Angew. Chem. Int. Ed.* **60**, 5083–5090 (2021).
40. Salter, M. W. & Stevens, B. Microglia emerge as central players in brain disease. *Nat. Med.* **23**, 1018–1027 (2017).
41. Peng, X. et al. Ultrafast self-gelling powder mediates robust wet adhesion to promote healing of gastrointestinal perforations. *Sci. Adv.* **7**, eabe8739 (2021).
42. Heallen, T. R. & Martin, J. F. Heart repair via cardiomyocyte-secreted vesicles. *Nat. Biomed. Eng.* **2**, 271–272 (2018).
43. Zhou, W.-t et al. Electrical stimulation ameliorates light-induced photoreceptor degeneration in vitro via suppressing the proinflammatory effect of microglia and enhancing the neurotrophic potential of Müller cells. *Exp. Neurol.* **238**, 192–208 (2012).
44. Gellner, A.-K., Reis, J., Fiebich, B. L. & Fritsch, B. Electrified microglia: Impact of direct current stimulation on diverse properties of the most versatile brain cell. *Brain Stimul.* **14**, 1248–1258 (2021).
45. Savina, A., Fader, C. M., Damiani, M. T. & Colombo, M. I. Rab11 promotes docking and fusion of multivesicular bodies in a calcium-dependent manner. *Traffic* **6**, 131–143 (2005).
46. Ma, Y. et al. Exosomal mRNAs for angiogenic-osteogenic coupled bone repair. *Adv. Sci.* **10**, 2302622 (2023).
47. Toita, R., Kang, J.-H. & Tsuchiya, A. Phosphatidylserine liposome multilayers mediate the M1-to-M2 macrophage polarization to enhance bone tissue regeneration. *Acta Biomater.* **154**, 583–596 (2022).
48. Li, X. et al. Dopamine-Integrated nanointerface between fibrillar matrix and hydrophilic nanohydroxyapatite regulates immune microenvironment to boost endogenous bone regeneration. *Adv. Funct. Mater.* **33**, 2212738 (2023).
49. Merx, M. W. et al. Transplantation of human umbilical vein endothelial cells improves left ventricular function in a rat model of myocardial infarction. *Basic Res Cardiol.* **100**, 208–216 (2005).
50. Qiu, X. et al. Exosomes released from educated mesenchymal stem cells accelerate cutaneous wound healing via promoting angiogenesis. *Cell Prolif.* **53**, e12830 (2020).
51. Zacchigna, S. et al. Paracrine effect of regulatory T cells promotes cardiomyocyte proliferation during pregnancy and after myocardial infarction. *Nat. Commun.* **9**, 2432 (2018).
52. Costa, Ambra et al. Investigating the paracrine role of perinatal derivatives: human amniotic fluid stem cell-extracellular vesicles show promising transient potential for cardiomyocyte renewal. *Front Bioeng. Biotechnol.* **10**, 902038 (2022).
53. Cahill, T. J. & Kharbanda, R. K. Heart failure after myocardial infarction in the era of primary percutaneous coronary intervention: Mechanisms, incidence and identification of patients at risk. *World J. Cardiol.* **9**, 407 (2017).
54. Wu, Y. et al. Exosomes rewire the cartilage microenvironment in osteoarthritis: from intercellular communication to therapeutic strategies. *Int. J. Oral. Sci.* **14**, 40 (2022).
55. Chen, Z. et al. Bioorthogonal catalytic patch. *Nat. Nanotechnol.* **16**, 933–941 (2021).
56. Wu, Q. et al. Advances in extracellular vesicle nanotechnology for precision theranostics. *Adv. Sci.* **10**, 2204814 (2023).
57. Zhang, J. et al. Programmed nanocloak of commensal bacteria-derived nanovesicles amplify strong immunoreactivity against tumor growth and metastatic progression. *ACS Nano* **18**, 9613–9626 (2024).
58. Wan, S. et al. Mechano-electronic stimulation of autologous extracellular vesicle biosynthesis implant for gut microbiota modulation. *Nat. Commun.* **15**, 3343 (2024).
59. Peng, F. et al. Nanoparticles promote in vivo breast cancer cell intravasation and extravasation by inducing endothelial leakiness. *Nat. Nanotechnol.* **14**, 279–286 (2019).
60. Tee, J. K. et al. Nanoparticles' interactions with vasculature in diseases. *Chem. Soc. Rev.* **48**, 5381–5407 (2019).

Acknowledgements

We thank Dr. M.W. in Suzhou Institute of Nano-Tech and Nano-Bionics, Chinese Academy of Sciences for the assistance of device establishment and J.J.Z. for her help in animal experiments. This work was supported by Natural Science Foundation (22207056 to X.G.D. and 62288102 to L.H.W.). This work was also supported by the CAS Key Laboratory of Nano-Bio Interface (21NB101 to X.G.D.), CAS Key Laboratory of Nanodevices and Applications (22ZS06 to X.G.D.) and Postgraduate Research & Practice Innovation Program of Jiangsu Province (SJCX23_0284 to S.Y.F.).

Author contributions

Z.Y.W., S.Y.F., and X.G.D. designed the study, prepared the figures, and wrote the manuscript. S.Y.F., Z.Y.W., P.H.H., G.J.L., J.N. and P.C.Z. performed the research. Z.Y.L, G.Y.Z., L.H.W, D.T.L. and X.G.D. analyzed the data. All authors contributed to the manuscript. S.Y.F., Z.Y.W., and P.H.H. contributed equally.

Competing interests

Authors declare no competing interests.

Additional information

Supplementary information The online version contains supplementary material available at <https://doi.org/10.1038/s41467-025-58260-0>.

Correspondence and requests for materials should be addressed to David Tai Leong or Xianguang Ding.

Peer review information *Nature Communications* thanks Elisa Garbayo, and the other, anonymous, reviewer(s) for their contribution to the peer review of this work. A peer review file is available.

Reprints and permissions information is available at <http://www.nature.com/reprints>

Publisher's note Springer Nature remains neutral with regard to jurisdictional claims in published maps and institutional affiliations.

Open Access This article is licensed under a Creative Commons Attribution-NonCommercial-NoDerivatives 4.0 International License, which permits any non-commercial use, sharing, distribution and reproduction in any medium or format, as long as you give appropriate credit to the original author(s) and the source, provide a link to the Creative Commons licence, and indicate if you modified the licensed material. You do not have permission under this licence to share adapted material derived from this article or parts of it. The images or other third party material in this article are included in the article's Creative Commons licence, unless indicated otherwise in a credit line to the material. If material is not included in the article's Creative Commons licence and your intended use is not permitted by statutory regulation or exceeds the permitted use, you will need to obtain permission directly from the copyright holder. To view a copy of this licence, visit <http://creativecommons.org/licenses/by-nc-nd/4.0/>.

© The Author(s) 2025